LIMNOLOGY and OCEANOGRAPHY

ASLO

Limnol. Oceanogr. 9999, 2020, 1–17

doi: 10.1002/lno.11670

Daily entropy of dissolved oxygen reveals different energetic regimes and drivers among high-mountain stream types

Marta Boix Canadell,[1] **Lluís Gómez-Gener**,[1] **Mélanie Clémençon**,[2] **Stuart N. Lane**,[2] **Tom J. Battin**[1*]

[1]Stream Biofilm and Ecosystem Research Laboratory, School of Architecture, Civil and Environmental Engineering, École Polytechnique Fédérale de Lausanne, Lausanne, Switzerland

[2]Institute of Earth Surface Dynamics (IDYST), University of Lausanne, Lausanne, Switzerland

Abstract

High-resolution time series of dissolved oxygen (DO) have revealed different ecosystem energetics regimes across various stream types. Ecosystem energetic regimes are relevant to better understand the transformation and retention of nutrients and carbon in stream ecosystems. However, the patterns and controls of stream energetics in high-mountain landscapes remain largely unknown. Here we monitored percent DO saturation (every 10 min) over 2 years in a glacier-fed, krenal (groundwater-fed) and a nival (snowmelt-fed) stream as they are typical for the high mountains. We used daily Shannon entropy to explore the temporal dynamics of stream water DO and to infer information on the ecosystem energetics and on the potential drivers. We found that discharge modulated the drivers of DO variations at daily and seasonal scales. Elevated bed movement along with high turbidity and very high gas exchange rates drove the daily DO patterns in the glacier-fed stream during snow and ice melt, whereas light seemed to drive DO dynamics in the krenal and nival streams. We found a window of favorable conditions for potential gross primary production (GPP) during the onset of the snowmelt in the glacier-fed stream, whereas potential GPP seemed to extend over longer periods in the krenal and nival streams. Our findings suggest how the energetic regimes of these high-mountain streams may change in the future as their biological and physical drivers change owing to climate warming.

Time-series of stream water dissolved oxygen (DO) can reveal patterns and processes of stream ecosystem energetics (Bernhardt et al. 2018). The temporal variation of stream water DO concentrations at diel and seasonal scales arises from the balance between biological and physical processes. In terms of physical processes, turbulence modifies DO availability across a range of time-scales, and the turbulence is generally a function of shear at the air–water interface boundary (Tamburrino and Gulliver 2002). In shallow streams, the air–water interface is strongly impacted upon by channel slope and bed roughness (Raymond et al. 2012; Ulseth et al. 2019). Steeper slopes increase water velocity which, in combination with bed roughness, can increase shear at the air–water interface, and hence turbulence, which is directly related to oxygen exchange (Zappa et al. 2007). There is a positive effect of temperature on the gas transfer velocity, which becomes negligible as turbulence increases (Demars and Manson 2013). In terms of biological processes, DO can be both produced, notably by gross primary production (GPP), and removed, notably by ecosystem respiration (ER). In high-alpine streams, most of the GPP is confined to benthic sediments, colonized by cyanobacteria, diatoms, *Hydrurus* and bryophytes, for instance. Ecosystem respiration involves both the respiration from the autotrophic and heterotrophic component of the benthic communities but also from the heterotrophic communities within the hyporheic zone (Naegeli and Uehlinger 1997; Battin et al. 2016).

Light availability, flow-induced disturbance and temperature count among the primary determinants of GPP and ER (Uehlinger and Naegeli 1998; Roberts et al. 2007). Variations in light regimes can come from shading by the riparian vegetation, stream water turbidity owing to suspended sediment, catchment topography and related variation in exposure to solar radiation (Julian et al. 2008). Besides light availability, streambed movement and scouring resulting from hydraulic forces acting on the sediments can constrain the accumulation of algal biomass with implications for GPP (e.g., Biggs et al. 1999; Uehlinger et al. 2002). Furthermore, the positive effect of temperature on GPP and ER is well established (e.g., Rasmussen et al. 2011), with ER expected to be more

*Correspondence: tom.battin@epfl.ch

Additional Supporting Information may be found in the online version of this article.

sensitive to changes in temperature than GPP (Enquist et al. 2003; Allen et al. 2005). Seasonal loadings of inorganic nutrients (e.g., nitrate, phosphate) and organic carbon can also fuel ER (Berggren and del Giorgio 2015).

The availability of reliable and affordable sensors now allows the study of the temporal dynamics of DO concentration and related environmental parameters at fine temporal resolution and over prolonged periods (Rode et al. 2016). In the last decade, time series of stream DO have been collected across different stream types with the purpose of understanding the temporal patterns of stream ecosystem metabolism and its drivers (e.g., Bernhardt et al. 2018; Appling et al. 2018*a*; Savoy et al. 2019). Processes that dominate stream water DO concentration are ultimately responsible of the DO regime typical for each stream or river, much as its energetic fingerprint (Bernhardt et al. 2018; Savoy et al. 2019). In large rivers in temperate zones, DO time series exhibit large daily DO variations resulting from enhanced GPP in summer (Dodds et al. 2015). In contrast, closed canopy reaches in headwater streams may impact DO dynamics such that peaks in DO concentration often mismatch the timing of potential light availability (Bernhardt et al. 2018). Furthermore, DO dynamics may also reflect the impact of stochastic flow-induced disturbance in low-order streams compared, for example, to the strong seasonality in larger and less frequently disturbed rivers.

In high-mountain streams, the melting of snow and glacial ice imparts a unique signature on the physicochemical properties of the stream water, including temperature, turbidity and related light attenuation, solute composition and concentration, as well as streambed stability (Robinson et al. 2002; Uehlinger et al. 2010; Gabbud et al. 2019). The interactions between these parameters over daily and seasonal scales create scenarios in which biological and physical processes play roles of alternating relevance in shaping stream ecosystem functioning. Thus far, despite the ubiquitous presence of high-mountain streams and their relevance for global biogeochemical fluxes (e.g., Horgby et al. 2019), we have limited understanding of the processes that regulate DO dynamics across temporal scales in these ecosystems. This poor understanding is remarkable given the profound climate-driven hydrological and physicochemical changes that these streams are facing. As the climate warms, depending on altitude, precipitation in spring and autumn will increasingly shift from snow fall to rain with major consequences on snow pack and runoff dynamics (e.g., Berghuijs et al. 2014). At the same time, mountain glaciers are shrinking (IPCC 2019), which further changes the magnitude and within-year distribution of runoff (Lane and Nienow 2019) and related physical and chemical parameters in glacier-fed streams (e.g., Milner et al. 2017). Implications of this unprecedented environmental change for ecosystem energetics in high-mountain streams remain largely elusive at present (Milner et al. 2017).

In this study, we aim to evaluate the effects of drivers, including light availability, streambed stability and gas exchange rate, to estimate the interactions between physical and biological processes that shape DO dynamics in high mountain streams: one glacier-fed (glacial), one groundwater-fed (krenal) and one snowmelt-fed (nival), in the Swiss Alps. To asses these interactions, we measured time series of DO saturation (%) every 10 min over 24 months. We derive Shannon entropy index to quantify daily patterns of stream water DO as was recently done for the temporal dynamics of discharge in a glacier-fed stream (Lane and Nienow 2019). Estimating GPP in highly turbulent streams with very high gas exchange rates is inherently difficult (e.g., Hall et al. 2015) as high reaeration can weaken the effect of GPP on DO dynamics and can lead to wrong metabolic estimates due to model equifinality (Appling et al. 2018*b*). Therefore, to explore a more conservative approach, we use DO entropy as an indicator for stream ecosystem energetics at daily and seasonal scales. We hypothesize that the relative importance of potential drivers, such as light and streambed stability, changes among the three stream types. We anticipate that the comparison of these drivers provides insights into the consequences of climate-induced environmental changes for high-mountain stream ecosystems.

Materials and methods

Study sites

Using the classification of Alpine streams types (sensu Brown et al. 2003), we study a glacial (Torrent du Valsorey, 28% glacier coverage), a krenal (Valsorey Spring) and a nival (Torrent de la Peule) stream in the Swiss Alps (Fig. 1; Table 1). All three streams drain catchments above the tree line where vegetation is predominantly primary colonizers, including grasses and shrubs (Supporting Information Table S1). Streams have steep slopes ($6.5 \pm 1.1\%$) and the streambed primarily composed of poorly sorted, coarse gravel and cobbles in the glacier-fed and nival stream. The streambed of the krenal stream was composed of finer sediments and was partially covered by large patches of bryophytes. Discharge follows temporal trends typical for high-alpine streams with extended base flow in winter when the streams are completely or partially snow covered, and with a marked snowmelt peak in spring followed by ice melt in the glaciated catchment in summer. All streams are also subject to the effects of summer rainfall (Fig. S1).

Baseline catchment characteristics

We identified and delineated the catchments using high-resolution (2×2 m) Swiss digital elevation model (DEM: swissALTI3D; Source: Geodata © swisstopo). We used the hydrology tool box in ArcGIS 10.3 (Environmental Systems Research Institute [ESRI]) to determine flow direction, flow accumulation and catchment boundaries. Land use coverage including glacier coverage within each catchment was based on the digital version of CORINE Land Cover inventory 2012 (© European Union, Copernicus Land Monitoring Service

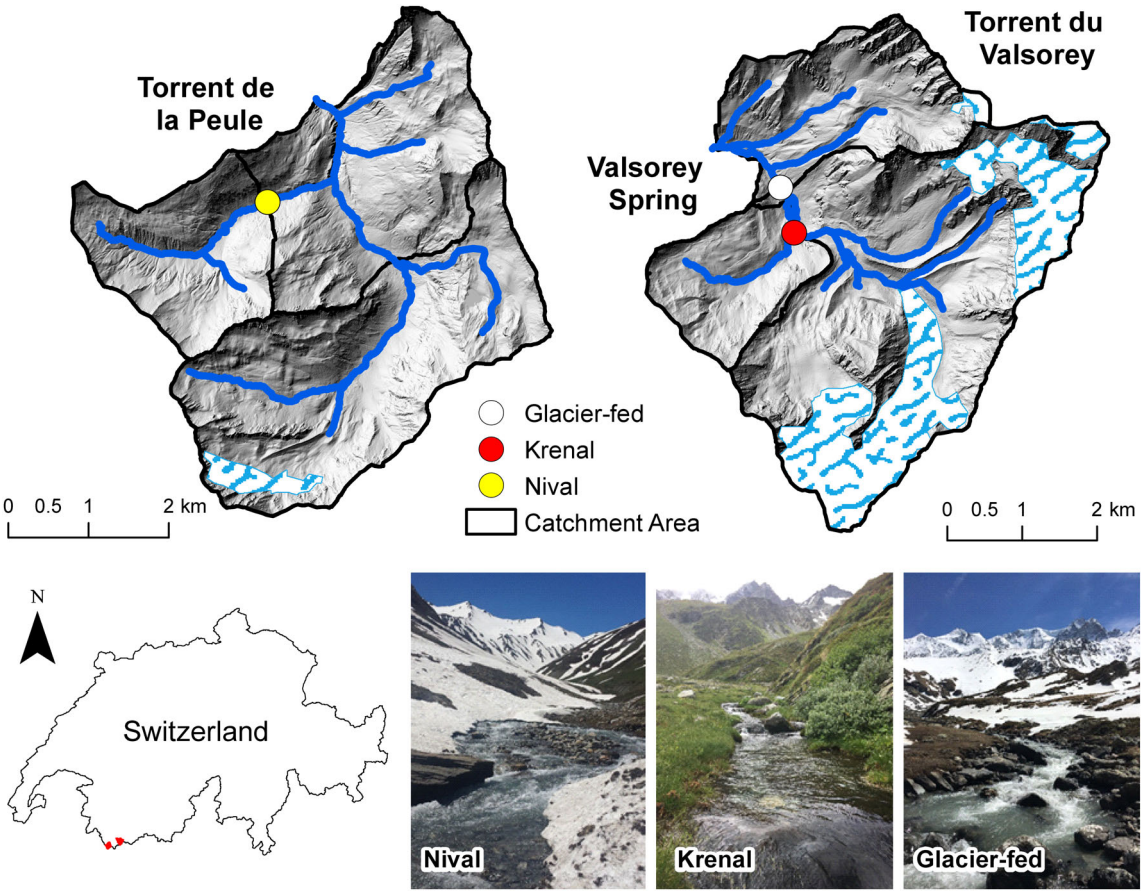

Fig. 1. Location of study streams and sensor stations in the Swiss Alps.

2018, European Environment Agency [EEA]) and the catchment boundaries previously delimited from the DEM.

Monitoring environmental parameters with sensors

At each stream, we deployed sensors to monitor stream water DO concentration (mg O_2 L^{-1}; accuracy ± 5% according to the manufacturer) and temperature (°C; miniDOT, Precision Measurement Engineering, Vista, California), turbidity (NTU; Cyclops-7 Turbidity, Turner Designs), and water depth (mm; Odyssey Capacitance Logger, Dataflow Systems Ltd). At each site we also monitored atmospheric pressure (mbar; Track-It™ Monarch Instrument) and light intensity measured as lux (lumens m^{-2}; Onset HOBO® Pendant) at the banks (1 m above ground). To accurately measure the light reaching the stream bottom, we installed additional light sensors at the stream bottom together with the turbidity and water depth sensors. We converted lux to photosynthetically active radiation (PAR; 400–700 nm) expressed as photosynthetic photon flux density (PPFD; μmol m^{-2} s^{-1}) by dividing lux by a constant value of 54 (Thimijan and Heins 1983).

Table 1. Summary of Catchment Characteristics of the Three Studied Streams.

Stream	Lat.	Long.	Altitude site (m a. s.l.)	Catchment Area (km^2)	Average Altitude Catchment (m a. s.l.)	Average Slope Catchment (degrees)	% Vegetated	% Bare Rocks	%Glaciers and Perpetual Snow
Glacier-fed	45.930	7.245	2148	18.1	2893 ± 399	31.4 ± 15.7	24	48	28
Nival	45.894	7.108	2027	4.0	2384 ± 157	29.5 ± 11.1	61	39	0
Krenal	45.928	7.246	2161	3.1	2548 ± 182	26.2 ± 12.6	65	35	0

All parameters were continuously recorded at 10 min interval from 15 October 2016 to 15 October 2018. We visited each stream approximately monthly for sensor maintenance and data downloading. During these visits, we measured stream water temperature and DO concentration with daily calibrated WTW multiparameter probes (Xylem Inc., USA). During winter, visits were less frequent because of high avalanche risk.

Spot gauging to estimate discharge (Q; $m^3\ s^{-1}$) for calibration of water level records was measured using slug-injections of sodium chloride as a conservative tracer (Gordon et al. 2004). Rating curves between water depth (z; m) and discharge were established for each site using a power-law model by fitting a linear regression on natural log transformed data (glacier-fed stream: $\log(Q) = 2.143\ \log(z) + 2.079$; $R^2 = 0.95$; $n = 7$; $p < 0.001$; groundwater-fed stream: $\log(Q) = 4.57\ \log(z) + 3.012$; $R^2 = 0.85$; $n = 10$; $p < 0.001$; nival stream: $\log(Q) = 1.539\ \log(z) + 1.752$; $R^2 = 0.93$; $n = 8$; $p < 0.001$). When data were missing because of depth sensor malfunctioning, we extrapolated gaps using least squares linear regressions with discharge data from sensors deployed in the same study area (Boix Canadell et al. 2019). Thereby, we reconstructed discharge data from 10 November 2016 to 7 June 2017 in the nival stream (total reconstructed 209 d; $R^2 = 0.84$; $p < 0.001$), from December 2016 to mid-May 2017 in the krenal stream (total reconstructed 165 d; $R^2 = 0.76$; $p < 0.001$) and from December 2016 to mid-May 2017 and from 10 August 2017 to 30 September 2017 in the glacier-fed stream (total reconstructed 217 d; $R^2 = 0.86$; $p < 0.001$). When extrapolation was not possible, variables derived from discharge (e.g., gas exchange rate, streambed movement) are missing as well. Occasional small gaps, with fewer than 4 d missing, were filled using linear interpolation.

Daily oxygen entropy

We estimated DO saturation concentration (i.e., the theoretical concentration of DO if the air and water temperature were at equilibrium; mg $O_2\ L^{-1}$) as a function of water temperature and atmospheric pressure using *calc_DO_sat* function from the *streamMetabolizer* R package (Appling et al. 2018*c*). The argument "model" was set to "Garcia-benson" which corresponds to a DO saturation concentration estimation based on Garcia and Gordon (1992). Later, we converted our measured DO concentration (mg $O_2\ L^{-1}$) to a percentage of atmospheric saturation (percent DO saturation). Next, daily entropy (E_d) of percent DO saturation was calculated using:

$$E_d = \frac{1}{n}\sum_{i=1}^{n}\frac{S_i}{\bar{S}_i}\log\frac{S_i}{\bar{S}_i} \quad (1)$$

where S_i is the percent DO saturation for time step i for n time steps within each day d and $\bar{S}_i$ is the average of S over n time steps within each day (d). Eq. (1) measures the extent of deviation within each day from the mean percent DO saturation for that day. A higher value of E_d indicates a greater range of diurnal variability of DO saturation as compared to the daily mean value. Essentially daily DO entropy informs on the departure of percent DO saturation from its baseline and is thus assumed to reflect biological (e.g., GPP) and physical (e.g., gas exchange) processes.

Gas exchange rate

For each stream, we estimated gas exchange rates (K600; d^{-1}) from argon tracer gas injections (Ulseth et al. 2019). Argon releases were conducted through the year to capture variability of the gas exchange coefficient during different flow conditions (i.e., base flow, snow, and glacier melt). Gas exchange rates for the entire study period were computed from stream specific log–log least-squared linear regressions between discharge data and K600 measured in the field. Discharge (Q; $m^3\ s^{-1}$) and velocity (v; m s^{-1}) were calculated from slug releases during the day of the gas injection. We measured stream channel width ($n = 10$) of the upstream reach and estimated mean stream depth assuming hydraulic continuity, that is, $\bar{z_{i,d}} = \frac{Q}{wv}$. Further details on the estimation of K600 and hydraulic geometry are provided in Ulseth et al. (2019).

PAR attenuation

For the periods where measurements of water depth data, turbidity and PAR at the stream bottom were available, we calculated coefficient of extinction of PAR (K_d, m^{-1}) rearranging the equation of the light attenuation function (Wetzel 2001; Supporting Information Eq. (S1)):

$$I_z = I_o \exp^{-K_d \times z} \quad (2)$$

where I_z is the PAR reaching the stream bottom, I_o is the PAR reaching the stream surface and z is the water depth (m). First, to calculate the coefficient of extinction, we used the water depth data recorded from the water depth sensor which was deployed next to the light sensor. Next, we related K_d with of the corresponding value of the stream water turbidity to obtain a K_d for each time step as a function of turbidity. Finally, we applied the light attenuation function with the turbidity-specific K_d to obtain the PAR at the stream bottom as a function of mean stream depth ($\bar{z_{i,d}}$) at each time point.

Modeling streambed stability

We used a 2D hydrodynamic model (Vetsch et al. 2018) to compute streambed stability using predicted shear stresses combined with sediment size distribution data to infer the relative proportion of the streambed with sediments moving owing to increases in discharge. We consider the relative proportion of the streambed in movement as a proxy for streambed stability. Streambed topography and grain size characterization from the reach upstream of our sensors was obtained from digital elevation models (DEMs) and high-resolution orthoimaginery using structure-from-motion photogrammetry and bathymetric correction due to the effects of

refraction in the water column (Dietrich 2017). Aerial photographs were taken during low flow (nival stream: 12 October 2017; krenal and glacier-fed streams: 13 October 2017) with a drone (SZ DJI Technology Co. Ltd.) equipped with a 12.4 megapixel camera. Image overlap was approximately 80% along the flight path, the drone was flown at two altitudes and the camera was set as off-nadir, so as to minimize the systematic error in acquired data. Before each flight, we marked ground control points spaced throughout the reach for posterior image georeferencing and determined their position to within a few centimeters using a Trimble real-time kinematic (RTK) GPS unit. All images were processed using Pix4D software (Pix4D SA). The resulting orthomosaics and DEMs had spatial resolutions between 1.24 and 1.28 cm/px and were georeferenced to the Swiss grid system (x, y) and mean annual sea level. Finally, we delimited and corrected wetted areas of generated DEMs for refractive effects as in Dietrich (2017).

Median sediment sizes were estimated with digital image processing of the high-resolution orthophoto (Carbonneau et al. 2004). Using ArcGIS 10.3, for each of the three rivers, 20 grids of 1 m × 1 m with 16 line intersections were evenly superimposed onto the image covering both wet and dry areas of the active channel. Within each grid, the intermediate b axis of pebbles which were at the line intersection was manually draw and its length (mm) automatically measured. The length of the b axis gave an estimate of median grain size (D_{50}) for each grid. We then apply a 1 m × 1 m moving window to the orthoimagery and calculate the semi-variance for different sub windows from 3 × 3 pixels to the $n \times n$ pixels corresponding to the size of the moving window. Tests suggested that the maximum semi-variance measured was strongly correlated with D_{50}. Thus the D_{50} measures were divided randomly into training and validating datasets. The training dataset was used to parameterize the relationship between grain size and semi-variance. This relationship was then applied to the orthoimagery for the river concerned to produce a map of D_{50}. These were validated using the second dataset and calculating mean and standard deviation of error (Supporting Information Table S5). The approach used to produce a D_{50} map needed only one modification for the krenal stream. The moss cover was estimated by the texture based D_{50} mapping to be sand and easily movable. Field observations suggested that these zones of moss cover were extremely stable. Thus, for the krenal reach, moss was mapped on the orthoimage and associated zones were labeled as permanently stable for the streambed stability modeling described below.

To obtain estimates of bed shear stress we used a method similar to that adopted for a similar type of stream (Gabbud et al. 2019) and a summary is provided here. We used the BASEMENT v2.7 hydraulic model (ETHZ, VAW, 2017), which solves the depth-averaged form of the Navier–Stokes equations for mass and momentum conservation using a finite element mesh (Vetsch et al. 2018). Turbulence was represented using a Reynolds decomposition with a zero-order eddy viscosity turbulence model. Bed shear stresses were represented using a quadratic friction law with a Manning roughness coefficient. In all the streams, Manning coefficient was set at 0.045 in all the streams as suggested for bedrock and gravel substrates based on calibration for similar streams in the region (Gabbud et al. 2019). Model solution used an exact Riemann solver and time steps were set automatically using the Courant–Friedrichs–Lewy condition. The downstream boundary used a depth-discharge relationship based upon the Manning equation and in all cases it was set downstream of the zone of interest in this study. In all model runs a steady discharge was applied at the upstream section and the model run to steady state, with the mass balance error (the difference between mass inflow rate and mass outflow rate) less than 0.5%.

The DEM of the channel bathymetry was resampled to 0.1 m resolution for the hydraulic modeling, a resolution that reflected a compromise between representation of topographic detail and computational efficiency. These data were converted into an unstructured triangular mesh using BASEmesh in the Quantum GIS software.

In all cases, the model was parameterized using Manning's n comparing inundated zones measured in the orthophoto with model predictions of inundation (Gabbud et al. 2019). Once the model was optimized, discharges were simulated every 0.1, 0.06, and 0.04 $m^3\ s^{-1}$ for the glacier-fed stream (n = 62), groundwater-fed stream (n = 46) and nival stream (n = 23) between the minimum and the maximum values of the range of discharge measured in each stream. All other parameter values were left constant. The bottom shear stress (τ_b) values predicted for each model run were then compared with a critical shear stress required for entrainment, using a Shields stress:

$$\tau_{oc} = 0.06(\rho_s - \rho)gD_{50} \quad (3)$$

where g is the gravitational constant, ρ_s the sediment particle density (kg m^{-3}), ρ the water density (kg m^{-3}), and D_{50} is the median of the particle size distribution extracted from the D_{50} map of the reach corresponding to the same hydraulic model grid cell. Application of this rule is supported by qualitative observations that the streambeds were poorly armored. For each reach, it was possible to calculate the percentage of the streambed that was mobile for each simulated discharge and the provided a look up table. By applying the look up table to the calibrated discharge record, we were able to transform the time series of discharge into a time series of streambed stability.

Statistical analysis

For each stream we identified the snow-free periods for both years by combining satellite images with field observations and by inspecting time series of percent DO saturation and its deviation from the winter baseline. In 2017, snow-free periods for the glacier-fed, nival and krenal streams started 6 April, 15 June, and 1 May and lasted 278, 154, and 253 d,

respectively. In 2018, there was a delay in the loss of the snow cover, the latter extending into summer in the catchment drained by the nival stream, that clearly reduced PAR at the stream bottom until 27 July. Glacier-fed and krenal streams lost the snow cover on 18 May and 1 June, respectively, in 2018. All three streams remained snow-free until the end of the study period.

To explore the effect of daily average of PAR, turbidity, K600, bed stability and discharge on DO entropy for the 2017 and 2018 snow-free periods, we conducted quantile regression analysis using the *quantreg* package in R (Koenker 2019). The use of quantile regression analysis allowed us to disregard the assumption of normal distribution and constant variance for the response. Also, it allowed us to focus on the effect of the explanatory variables on the highest values of the frequency distribution (i.e., 90th percentile regression). The *quantreg* package requires a sample size of at least 1000 to calculate *p* values but can calculate the slope and intercept of regressions with smaller samples sizes. We were not able to determine significance for the different relationships but report the slope and intercept results to show the general trends. We report the 95% confidence intervals as a measure of variability of the estimated quantile regression coefficients. Streambed movement (%) was arcsine-square-root transformed for quantile regression analyses.

Additionally, we applied for each stream individually a partial least squares regression (PLS) analysis to explore how daily average of PAR, turbidity, K600, bed stability and discharge predict daily DO entropy during the 2017 snow-free period. PLS identifies the relationship between independent (X) and dependent (Y) data matrices through a linear, multivariate model and produces latent variables (PLS components) representing the combination of X variables that best describe the distribution of observations in "Y space" (Eriksson et al. 2006). We determined the goodness of fit (R^2Y) and the predictive ability (Q^2Y) of the model by comparing modeled and actual Y observations through a cross validation process. We identified the importance of each X variable by using variable importance on the projection (VIP) scores, calculated as the sum of square of the PLS weights across all components. VIP values > 1 indicate variables that are most important to the overall model (Eriksson et al. 2006). The PLS was fitted using the *plsr* function from the R package *pls* (Mevik et al. 2019). We dealt with temporal autocorrelation of the data by detrending and differencing the time series of both dependent and independent variables using the R package *forecast* (Hyndman et al. 2019). The effect of the two transformations on the temporal autocorrelation of the data was visually assessed by exploring ACF correlograms before and after transformation (Supporting Information Figs. S2–S4). Data pre-processing for PLS analysis also included the arcsine of the square root of % of streambed movement and the data standardization of all variables. Ultimately, the number of days available for quantile regression and PLS analysis for 2017 were n = 277 d (glacier-fed stream), n = 124 d (nival stream) and n = 251 d (krenal stream). The number of days used in the quantile regression analyses for the year 2018 were 147, 79, and 116 for the glacier-fed, nival and krenal stream respectively. Additionally, to better define windows with potential good conditions for primary production in the glacier-fed stream, we tested for abrupt shifts in the variance of discharge, turbidity, bed movement and also DO entropy by implementing a change point analysis using the *changepoint* R package (Killick et al. 2016). Change point analysis was performed for the year of the PLS analysis (2017). Finally, we described the relationship between relative streambed movement (transformed by the arcsine of the square root) and discharge using a general power-law function defined as $y = ax^b$. All statistical analyses were conducted in *R* (version 3.6.1) except entropy calculations that were conducted using MATLAB (The Mathworks Inc., Natik, Massachusetts).

Results

Physical template of alpine streams

The annual dynamics of the physical template potentially relevant to ecosystem metabolism differed markedly among our three study streams (Fig. 2). The hydrological regime of the glacier-fed stream was characterized by distinct snowmelt in spring and glacial melt in summer with a median discharge of 0.28 $m^3\ s^{-1}$ during the study period. The groundwater-fed and the nival streams had slightly differing hydrological regimes from the glacier-fed stream and with lower median discharge (0.01 and 0.08 $m^3\ s^{-1}$, respectively). Snowmelt discharge in the krenal stream differed between years, an observation consistent with the greater snow pack during the 2017/2018 winter across western Alps (Stoffel and Corona 2018).

Streamwater turbidity was often high in the glacier-fed stream during summer (values of 1712 and 2500 NTU in July 2017 and 2018, respectively) and related to discharge (R^2 = 0.54; $p < 0.001$). Turbidity was generally low in the krenal (median: 1.5 NTU) and nival (median: 1.2 NTU) streams and occasionally peaked with increases in discharge; however, discharge did not explain the variability of turbidity on an annual basis in these streams (krenal: $R^2 = 8.86 \times 10^{-5}$; p = 0.003; nival: R^2 = 0.02; $p < 0.001$). Both water depth and turbidity affected PAR attenuation within the stream water. In the glacier-fed stream, daily mean of radiation (median: 44 μmol photons $m^{-2}\ s^{-1}$) reaching the stream bottom was as low as 0.18 μmol photons $m^{-2}\ s^{-1}$ and 0.27 μmol photons $m^{-2}\ s^{-1}$ in August 2017 and 2018, respectively. Owing to reduced turbidity and shallower stream water, daily mean of radiation near the stream bottom was generally higher in the krenal (median: 204 μmol photons $m^{-2}\ s^{-1}$) and nival (median: 400 μmol photons $m^{-2}\ s^{-1}$) streams during the two snow-free periods.

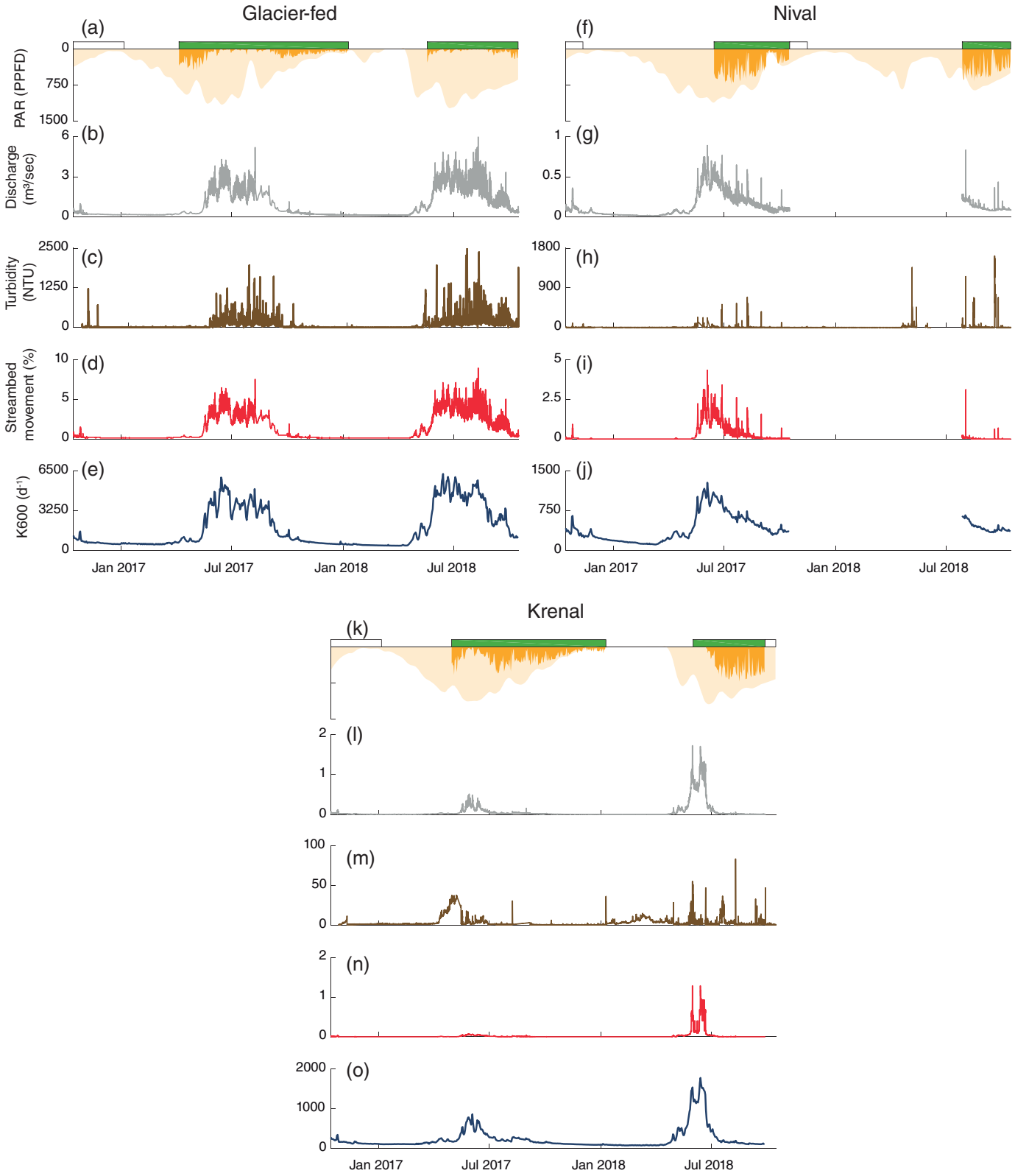

Fig. 2. Legend on next page.

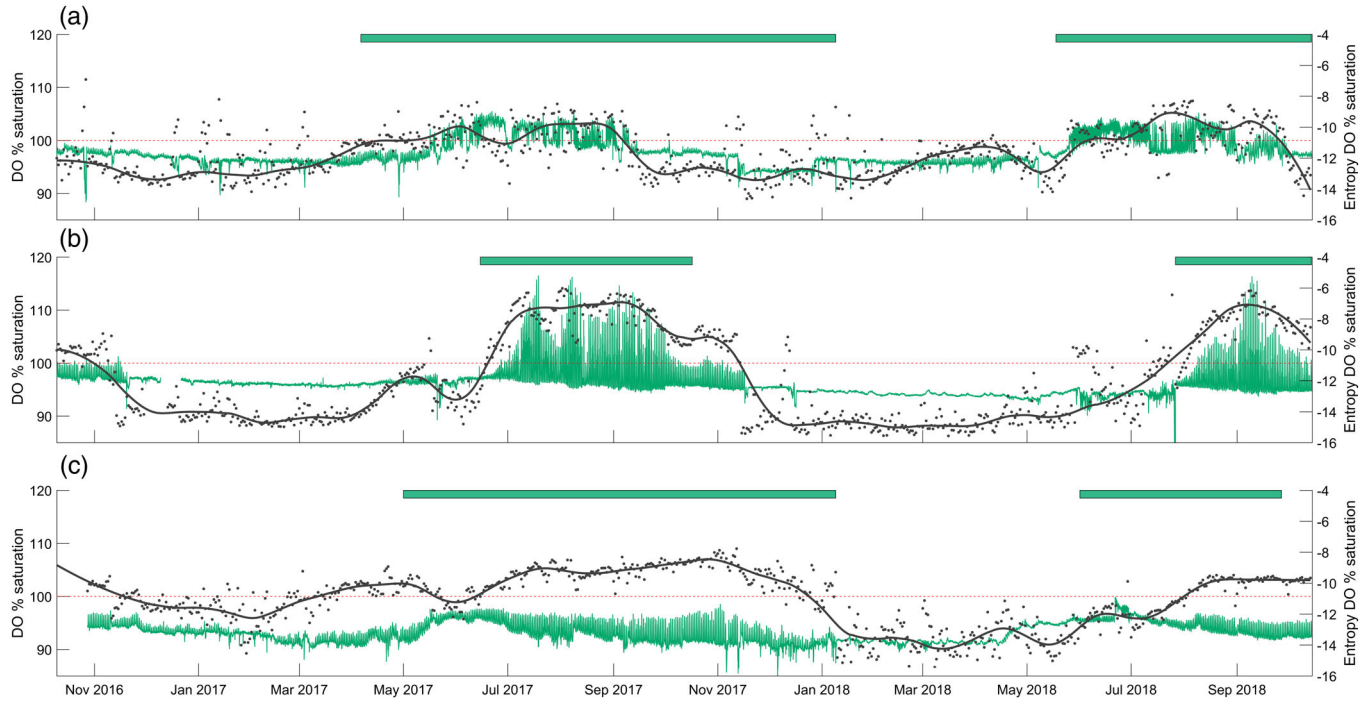

Fig. 3. Time series of dissolved oxygen (DO) % saturation (green) at 10-min frequency, daily entropy DO% saturation (dots) and smoothing filter applied on oxygen entropy data (line; Matlab smooth function: Span = 0.01 and method = rloess). (**A**) Glacier-fed, (**B**) nival, and (**C**) Krenal. Oxygen entropy is natural log transformed for representation purposes. Dashed red line shows 100% saturation limit. See caption Fig. 2 for explanation of the bars above each plot.

On an annual basis, streambed movement was significantly higher in the glacier-fed stream (median: 0.2%; range: 0.12–8.9%; Kruskal–Wallis and pairwise Wilcoxon test $p < 0.001$) than in the krenal (median: 0%; range: 0–1.3%) and nival (median: 0%; range: 0–4.3%) streams. Not unexpectedly, elevated streambed movement was clearly related to increased runoff from snowmelt and ice melt. The coefficient (b) of the power-law used to describe the relationship between relative streambed movement and discharge varied among streams. The coefficient was lowest (0.61; 95% CI: 0.60, 0.62) in the glacier-fed stream despite its high streambed movement; it was 0.86 (95% CI: 0.83, 0.89) in the krenal and 1.52 (95% CI: 1.48, 1.56) in the nival stream.

Owing to the highly turbulent character of the glacier-fed stream, we found very high gas exchange rates in this stream (median: 841 d^{-1}), with potential maxima as high as 6273 d^{-1}. Over the year, median gas exchange rates were lower in the krenal (median: 133 d^{-1}) and nival (median: 363 d^{-1}) streams and, as expected, clearly driven by changes in discharge. Average gas exchange among streams was not in line with streams slope (5.9%, 5.8%, and 7.7% for the glacier-fed, nival and krenal streams).

Finally, change point analyses in the glacier-fed stream detected shifts in the temporal dynamics of discharge, bed movement and turbidity (Supporting Information Fig. S5). Both time series of discharge and bed movement showed a change in variance in 2017 on 23 May and 1 September and additionally on 15 October in discharge data. Changes in turbidity were detected on 2 June 2017 and 1 September. Changes in DO entropy were identified on 22 May and 6 September.

FIG. 2. Time series of environmental data in (**A**)–(**E**): Glacier-fed, (**F**)–(**J**): nival, and (**K**)–(**O**): Krenal streams. Bars above plots (**A**), (**F**), and (**K**) represent snow-free periods. Green bars represent periods analyzed with quantile regression (2017 and 2018) and partial least squares regression (PLS) analysis (2017). White bars represent snow-free periods where data has not been analyzed because either was not the scope of the study (i.e., winter 2016) or because missing data (i.e., 2017 in nival stream and 2018 in krenal stream). No bars represent snow-covered periods. Photosynthetically active radiation (PAR) reaching the stream surface is shown in light yellow. PAR reaching the streambed bottom for the studied periods is shown in dark yellow. Discharge, turbidity and % streambed movement represented at 10 min frequency. PAR (as PPFD; μmol m^{-2} s^{-1}) and gas exchange rates (K600) data represented by daily means.

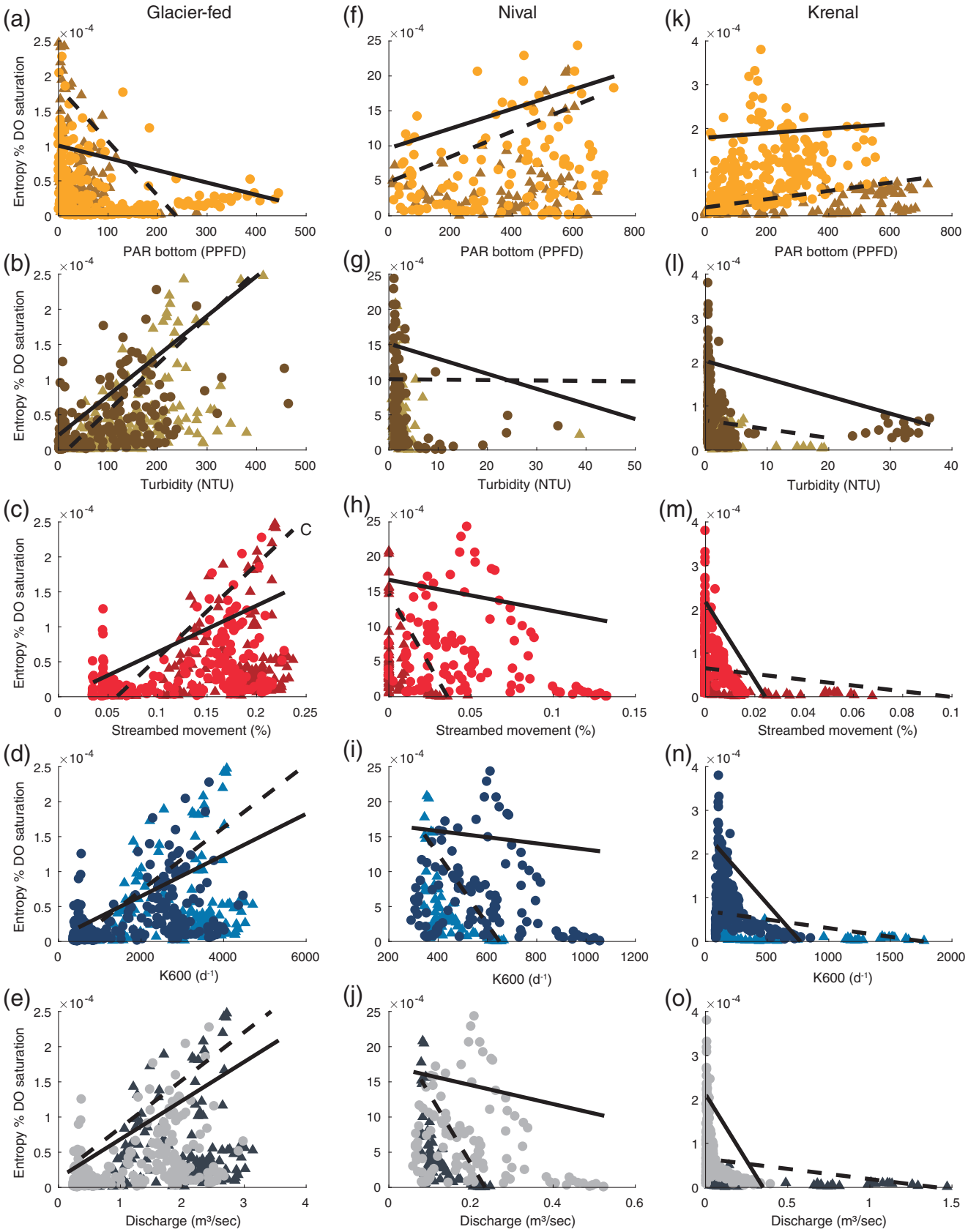

Fig. 4. Legend on next page.

Dynamics and entropy of DO saturation

The continuous monitoring of streamwater DO revealed distinct temporal trends in oxygen saturation in all three study streams (Fig. 3). During snow cover, median oxygen saturation was below saturation (glacier-fed: 96%; krenal: 92%; nival: 95%) reaching minimum values of 90%, 78%, and 87% in the glacier-fed, nival and krenal streams, respectively. Its diel variation (as the coefficient of variation, CV) was 0.7% (glacier-fed), 1.3% (nival), and 1.5% (krenal) reaching maximum values of 99%, 99%, and 96% in the glacier-fed, nival, and krenal stream, respectively. Despite the very low variation in oxygen saturation during the snow cover, it is reasonable to conclude that oxygen saturation was lowest in all three streams during that period. With the first stages of the snowmelt and the following snowmelt peak, stream water oxygen saturation markedly increased (above 100% saturation) in the glacier-fed and nival streams, with maximum values of 106% and 117% respectively. During that same period, the diel variations in oxygen saturation increased as well in the glacier-fed (median: 98%; CV: 2.8%) and nival (median: 97%; CV: 3.5%) streams, particularly in that former. These dynamics differed in the krenal stream. Here stream water oxygen consistently remained below saturation (median: 94%; maximum: 99%) and yet it depicted clear diel swings (CV: 2%).

Our entropy approach, which essentially describes the departure from the baseline over 24 h periods, captured the diel variation in oxygen saturation well, and even on an annual scale (Fig. 3). Low baseline oxygen saturation combined with reduced diel departures translates into low daily entropy values during snow cover (median for glacier-fed stream: 4.7×10^{-6}; (log: −12.2), krenal stream: 3.2×10^{-6}; (log: −12.6), and nival stream: 6.4×10^{-7}; (log: −14.3)). Daily entropy increased with the loss of the snow cover and the onset of the snowmelt and remained elevated throughout spring and early summer in all three streams. The nival stream (median: 0.0002; [log: −8.1]) had highest daily entropy, followed by the krenal (median: 5.5×10^{-5}; (log: −9.8) and the glacier-fed (median: 1.7×10^{-5}; (log: −10.9) stream.

Potential drivers of the daily oxygen entropy

The effect of the different explanatory variables on daily oxygen entropy varied among streams and was captured by the slope of the quantile regression (Fig. 4; Supporting Information Tables S2–S4). In the glacier-fed stream, daily oxygen entropy positively and consistently related to discharge and related variables (i.e., turbidity, bed movement and gas exchange rate). Despite the heavily skewed distribution of the data (e.g., turbidity, gas exchange rate), these relationships were inverse in both the krenal and nival streams. The relationship between daily oxygen entropy and PAR at the stream bottom differed among streams. It was negative in the glacier-fed stream, positive in the snow-fed stream, while no real trend was detected for the krenal stream. We found that the observed trends were generally reproducible between both years, despite smaller sample sizes in 2018.

The partial least squares regression (PLS) analysis identified turbidity, bed activity, gas exchange rate and discharge as predictors (VIP > 1) of daily oxygen entropy in the glacier-fed stream ($R^2Y = 0.20$; $Q^2Y = 0.17$) (Fig. 5). The regression coefficients show a positive effect of these four variables and a negative but non-significant effect of PAR on daily oxygen

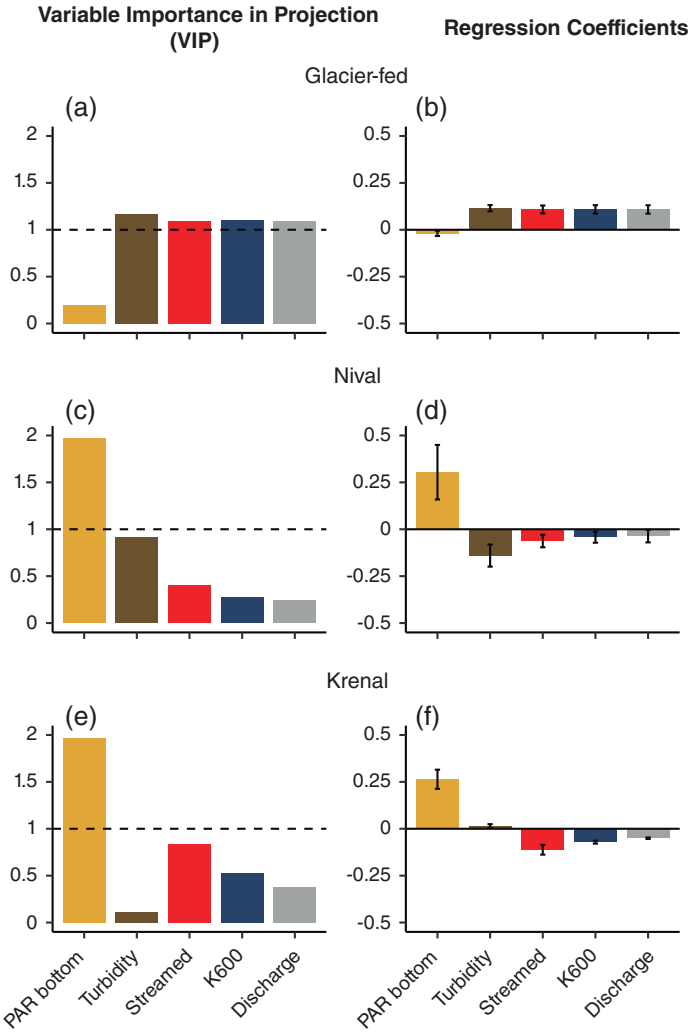

Fig. 5. Results from partial least squares regression (PLS) analysis. (**A**) and (**B**): Glacier-fed; (**C**) and (**D**): nival; (**E**) and (**F**): Krenal. Error bars represent the standard error of the regression coefficient estimates.

FIG. 4. Relationships between daily entropy and the daily average of different explanatory variables for both 2017 (circles) and 2018 (triangles). Lines represent 90th percentile regression for 2017 (continuous) and 2018 (dashed). (**A**)–(**E**): Glacier-fed stream, (**F**)–(**J**): nival stream, (**K**)–(**O**): Krenal stream. Note differences in *Y*-axis scales across streams. PAR as PPFD (μmol m^{-2} s^{-1}).

entropy. Conversely, PAR explained most of the observed variation in daily oxygen entropy in the two non-glacier fed streams (Fig. 5)., with elevated daily oxygen entropy primarily positively related to PAR (coef = 0.26; VIP = 1.96) in the krenal stream. Furthermore, the PLS model (R^2Y = 0.26; Q^2Y = 0.24) also revealed bed movement as a control (with a negative effect) on the daily oxygen entropy (coef = −0.11; VIP = 0.83) in the krenal stream. In the nival stream, PAR (coef = 0.30; VIP = 1.97) was positively related to daily oxygen entropy whereas turbidity (coef = −0.14; VIP = 0.9) was inversely related to daily oxygen entropy (R^2Y = 0.30; Q^2Y = 0.24).

Discussion

While climate and associated light and hydrologic regimes are understood as first-order controls on metabolic regimes, the combined effects of these physical controls (and their derivatives) with biological processes on stream metabolism are poorly understood to date. In this study, we found discharge as a major modulator of light availability at the stream bottom or gas exchange rate, all parameters that drove seasonal and daily DO variations. Our findings highlight the distinct temporal trends of DO in streams and eventually the differing energetic regimes across three typical alpine stream types.

Timing and magnitude of stream water DO

The discharge of alpine streams is typically very low from the end of autumn to the beginning of the snowmelt in spring, when channels are partially or completely covered by snow, or even frozen (Ward 1994). Consistent with this seasonal variation, our study streams remained snow-covered throughout winter when we registered the lowest percent of DO saturation values. Low DO saturation may relate to major infiltration of groundwater, typically low in DO, and sustaining base flow during the snow-covered period (e.g., Riley and Dodds 2013; Horgby et al. 2019). Also, as suggested by the lower daily DO entropy, snow-covered streams seemed to enter a "dormant period" during which no major biophysical processes deviate oxygen saturation from the groundwater-imposed baseline.

Groundwater discharge domination is supported by the median values of stream water electrical conductivity during these periods (glacier-fed stream: 289 μS cm^{-1}; krenal: 241 μS cm^{-1}; nival stream: 599 μS cm^{-1}; unpublished data), which are comparable to other studies (Brown et al. 2007; Horgby et al. 2019) and higher than during the snow-free periods (glacier-fed stream: 180 μS cm^{-1}; krenal: 205 μS cm^{-1}; nival stream: 527 μS cm^{-1}; unpublished data). Streamwater DO started to show different dynamics when stream flow became relieved from dominant groundwater inputs and snowmelt, for instance, started to contribute to the rising discharge. The response of DO varied in accordance with the physical template encountered within each stream and determined, for the most part, by the hydrological regime. Elevated discharge as sustained by snow and ice melt increases PAR attenuation and physical disturbance which are both unfavorable for the benthic algae in the glacier-fed stream (Malard et al. 2006; Uehlinger et al. 2010). At the same time, increasing discharge also increases turbulence and hence the gas exchange through the water surface. Thus, the onset of snowmelt supplies the stream with oxygen because the groundwater-dominated stream flow (low in oxygen and low turbulent regime) starts to equilibrate with atmospheric oxygen, facilitated by increasingly patchy and thinner snow cover. Surface runoff, enriched in oxygen itself, further contributes to the oxygen balance in the streams. The initial stages of snowmelt also constitute a "window of opportunity" (Battin et al. 2004; Uehlinger et al. 2010) with low turbidity and hence elevated PAR for primary producers which may increase the daily amplitude in oxygen saturation.

Potential drivers of DO dynamics

Glacier-fed stream

Both quantile regression and partial least squares regression (PLS) analysis revealed physical processes as the dominant control on oxygen dynamics in the glacier-fed stream. Very high discharge during snowmelt and particularly during ice melt in summer markedly influence the stream environment with impacts on percent DO saturation and its daily entropy. During these periods, the higher discharge, which is likely to increase turbulence, drastically increased the gas exchange rate (up to 6000 d^{-1}). This enhancement in gas exchange likely drives the observed enrichment in stream water oxygen after winter, as well as the constant daily oscillation of percent DO saturation values around 100% during high discharge. In fact, we argue that high values of daily oxygen entropy are linked to diurnal changes in discharge owing to the dynamics of snowmelt and glacier melt occurring during the period defined by abrupt changes in discharge from May to September in 2017.

It is now increasingly understood that bubble mediated-gas exchange is typical for high-mountain streams (Ulseth et al. 2019). High discharge in combination with the macroroughness of mountain streambeds increases turbulence to the point where the water surface continuously breaks and air is advected into the stream water, dramatically increasing the perceived oxygen saturation concentration (Zappa et al. 2007).

Flow-induced disturbance through bed scouring or local abrasion of biomass is a major control on the temporal and spatial dynamics of stream primary producers (Biggs et al. 1999). During high flow events, as shear stress exerted on the streambed rises towards the critical shear stress, coarser bed material is progressively mobilized thereby initiating bed scouring and transport (Biggs et al. 1999). Yet, even if there is not sufficient energy to move bedload, the shear stress applied to the benthic communities may be sufficient to scour

biomass (e.g., Bond and Downes 2003; Katz et al. 2018). Our geomorphological analysis of the streambed suggests that both snowmelt and glacier-melt were critical in reworking the streambed in the glacier-fed stream. Streambed stability is influenced by the combination of the flow regimes, sediment size distribution, channel slope and riparian vegetation (Duncan et al. 1999; Schwendel et al. 2010).

In high-mountain streams, bed roughness is typically higher than in low-gradient streams, with consequences for energy dissipation and the threshold of sediment movement (Schneider et al. 2015). A greater energy demand for sediment movement suggests that streambeds are less frequently mobilized in steep mountain streams than in low-gradient streams (Montgomery and Buffington 1997; Church 2006). For the case of the glacier-fed stream studied here, high rates of sediment supply and turnover appear to be sufficient to prevent the development of armor and keep resistance to entrainment relatively low. These sediment dynamics coupled with high discharge during snow and ice melt, would maintain elevated levels of streambed instability (Lane et al. 1996; Mao and Lenzi 2007). Extended periods of snow and ice melt significantly contribute to the annual bed load in nival and glacier-fed streams (e.g., Lane et al. 2017). This high rate of bed perturbation is likely to inhibit the development of benthic life in these streams (Uehlinger et al. 2010; Segura et al. 2011) and hence the GPP typical of more stable streams.

Besides inducing streambed movement, snowmelt and specifically ice melt can also mobilize fine sediments within the glacier forefield and its moraine depositions, which can drastically augment stream water turbidity at both seasonal and daily time scales (Lane et al. 2017; Milner et al. 2017). High loads of fine suspended solids in the stream water can constrain GPP via two mechanisms. On the one hand, abrasion by fine particles is a dominant physical mechanism removing periphyton (Hoyle et al. 2017). On the other, light within the stream water is attenuated by the absorption and scattering by fine particles (Julian et al. 2008). It was shown, for instance, that high turbidity similar to that measured in the glacier-fed stream significantly lowered benthic GPP in the Colorado River, Grand Canyon, (Hall et al. 2015). The negative impacts of discharge and related turbidity on benthic algal biomass and GPP have been well documented in various other glacier-fed streams (Uehlinger et al. 1998; Battin et al. 2004; Rott et al. 2006). Several studies have revealed the initial stages of snowmelt and a short period in fall as "windows of opportunities" for benthic algal biomass and GPP as discharge and turbidity were low, streambed stable, and both temperature and UV radiation moderate during these periods (e.g., Battin et al. 2004; Uehlinger et al. 2010).

In this context, we suggest for the glacier-fed stream that the increase in oxygen saturation along with higher daily entropy from the onset of snowmelt as channels become snow-free until the big change in discharge, bed movement and turbidity in May 2017 is a consequence of increasing GPP. As the melt season progresses, high levels of streambed movement coupled with reduced PAR availability likely impeded periphyton accrual and GPP. Therefore, we argue that physical drivers of DO dynamics prevailed over biological drivers during that period. However, it is noteworthy that in the event of GPP during that period, high gas exchange rates would have masked its effect on the oxygen dynamics variations (e.g., Guasch et al. 1998).

As ice melt recedes in September, a decrease in both oxygen concentration and daily entropy indicates poor recovery of potential GPP in both consecutive years in the glacier-fed stream. Based on oxygen dynamics, the lack of recovery contrasts with the autumnal window of opportunity observed in other glacier-fed streams (Uehlinger et al. 1998; Battin et al. 2004; Uehlinger et al. 2010). However, in glacier-fed streams, massive losses of benthic biomass during high flow in summer are often related to significant scouring (e.g., Rott et al. 2006). The recovery of benthic algal depends on the intensity of the flow-induced disturbance (Peterson et al. 1994; Segura et al. 2011; Katz et al. 2018). In this sense, recovery of algal biomass and GPP photosynthetic rates following bed movement are influenced by other environmental factors such as temperature or light (Uehlinger and Naegeli 1998; Uehlinger 2000; Segura et al. 2011). Our results suggest that the biomass potentially accumulated during the onset of snowmelt may have been lost, attributable to the prolonged disturbance throughout the melting seasons and to lack of favorable conditions thereafter.

Krenal and nival streams

During the snow-free periods and for both years, daily DO entropy followed the temporal variation of PAR at the stream bottom in both krenal and nival streams. Notably in 2017, we identified PAR as a major driver of the daily DO entropy in both streams, which suggests important contributions from GPP to the observed DO patterns. Due to the low turbidity in these two streams, water depth from the snowmelt peak was likely the main controller of PAR extinction during the snow-free period. As summer progresses into fall, base flow decreased and stream water became clearer. Thus, the reduction in PAR availability during the fall period was because of the lower angle of incident light, related mountain shading and reduction of day length. In the krenal stream, highest daily DO entropy was not associated with highest of PAR in 2017 after the snowmelt. Shallow and clear stream water along with relatively high PAR prevalent in high-altitude regions may have inhibited photosynthesis as shown experimentally in high-Alpine streams (Wellnitz and Ward 2000). By definition, higher daily oxygen entropy reflects either an increase in the magnitude of the daily percent DO saturation and or a decrease in the magnitude of the daily percent DO saturation minimum. In this manner, an increase in daily oxygen entropy as summer progresses may be a consequence of the gradual shift towards low-oxygen groundwater dominated

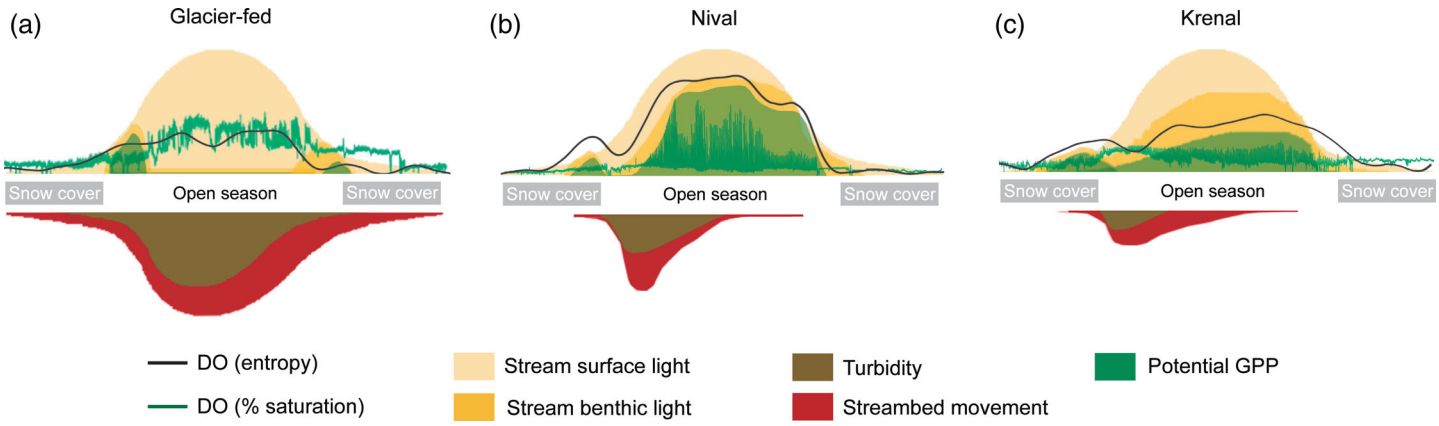

Fig. 6. Conceptual model of three annual energetic regimes for streams with contrasted physical and hydrological regimes typical for high-alpine catchments: a glacier-fed (**A**), a nival (**B**), and a krenal stream (**C**). The measured annual dissolved oxygen (DO) regimes (as both percentage of saturation and entropy) are the green and black lines, respectively. The annual pattern of potential solar radiation (i.e., radiation reaching the stream surface) is shown in light yellow while the actual incident solar radiation (i.e., radiation reaching the streambed bottom) in dark yellow. The annual patterns associated to physical disturbances (i.e., turbidity and streambed movement) are shown in brown and red, respectively. In high-alpine streams, the interplay of both light and disturbance regimes drives the timing, magnitude and extent of productivity periods occurring at annual basis (i.e., maximum potential for gross primary production (GPP)).

streamflow. In parallel, oxygen-consuming processes such as heterotrophic respiration in the stream surface and hyporheic sediments may further reduce the oxygen concentration.

In the nival stream, we did not find any indications of photoinhibition during the highest values of PAR measured at the streambed during the snow-free period. In fact, a reduction in PAR late in the season appears to have an immediate negative effect on both oxygen concentration and daily DO entropy. Of the three study streams, the nival stream showed the most immediate response of streambed movement to increasing discharge. However, oxygen production in this stream seemed to respond more negatively to a reduction on PAR due to high-turbid events rather than to streambed disturbance. We suggest that during bedload events, with the absence of major turbidity, primary producers colonizing more stable patches of the streambed can potentially maintain oxygen production. On the contrary, high-turbidity events with or without associated bedload may have an integral effect on the extinction of PAR that affects the entire stream bottom.

What makes the energetic regime in Alpine streams different?

Recent studies have revealed the seasonal patterns of ecosystem energetics across a broad range of streams (Bernhardt et al. 2018; Savoy et al. 2019). Using classifiers related to catchment characteristics and discharge, for instance, Savoy et al. (2019) identified two typologies of energetic regimes: streams with a peak productivity in spring or in summer. Such classifiers ultimately relate to the drivers of GPP, including light availability, as rooted in the River Continuum Concept (Vannote et al. 1980). Thus, the riparian canopy can reduce PAR) reaching small streams draining forested catchments and hence their GPP, whereas water depth and turbidity suppress PAR and GPP further downstream (Vannote et al. 1980). Blaszczak et al. (2019) have recently shown stream water turbidity as a modulator of GPP in urban streams through the attenuation of light reaching the streambed.

Based on daily (DO entropy, our study expands the current list of stream energetics regimes, and sheds light on their drivers, including light and streambed movement (Fig. 6). In fact, in high-mountain streams above tree line, snow cover during winter, stream water depth and turbidity, particularly during snow and ice melt in spring and summer, were major controls on PAR that reaches the bottom of three typical alpine streams. When periods of elevated PAR at the stream bottom were coupled with reduced bed movement, potential windows of opportunities emerged for GPP in spring but less so in fall in the glacier-fed stream. Between these windows, massive bed movement and turbidity depressed GPP such that no clear patterns in percent DO saturation and daily entropy emerged, except those that we attribute to daily changes in gas exchange rates, themselves modulated by fluctuations in discharge. Apparent ecosystem energetics in the nival stream followed the light regime outside the channel more closely because of low turbidity, and may hence be classified as a summer peak regime (sensu Savoy et al. 2019) with a minor peak during the snowmelt. The energetic regime in the krenal stream was shaped by an early and minor peak of apparent GPP during the onset of the snowmelt when turbidity was low and by an extended period of elevated apparent GPP after snowmelt when both bed movement and turbidity were low.

Our findings suggest that in the high mountains, earth processes, such as glacier dynamics and sediment production and

discharge modulate stream ecosystem energetics. Climate change is predicted to have major impacts on these modulators, particularly on glacier-fed streams that, as glaciers shrink, will shift towards nival and krenal-type ecosystems (e.g., Milner et al. 2017). Our comparative study suggests that this climate-driven transition in hydrology will also impact the energetics of these streams. We propose that, the favorable conditions (light, streambed stability) will extend towards early spring and late summer in krenal and nival streams due to an earlier and weaker snowmelt with reduced snowpack. Furthermore, glacier runoff beyond "peak water" (e.g., Huss and Hock 2018) in combination with reduced snowpack will decrease the discharge during spring and summer, but also on a diurnal scale (Lane and Nienow 2019), and hence both the magnitude and duration of the flow-induced disturbance. A gradual decrease in glacial melt volume and the magnitude of diurnal flow peaks will reduce bed scouring and sediment transport and it remains to be seen whether these reductions are sufficient to reduce levels of turbidity and so increase GPP in the glacier-fed streams. Eventually, however, clear groundwater will come to dominate summer runoff in these streams, thereby enhancing PAR penetration to their bottom. Consequently, benthic algal biomass may increase with a knock-on effect on benthic fauna community composition (e.g., Cauvy-Fraunié et al. 2016) or on bryophytes that may even outcompete benthic algae (Milner et al. 2017). However, groundwater may not be able to sustain streamflow, increasing periods of intermittency with potentially detrimental consequences for primary producers in these streams. Such shifts in ecosystem energetic regimes will have consequences for the temporal dynamics of carbon and nutrient transformation and retention. It is intuitive to assume that extended periods of GPP in high-mountain streams will reduce the downstream transport of nutrients, particularly phosphate, with yet unknown consequences for the downstream ecosystems.

REFERENCES

Allen, A. P., J. F. Gillooly, and J. H. Brown. 2005. Linking the global carbon cycle to individual metabolism. Funct. Ecol. **19**: 202–213. doi:10.1111/j.1365-2435.2005.00952.x

Appling, A. P., J. S. Read, L. A. Winslow, et al. 2018*a*. The metabolic regimes of 356 rivers in the United States. Sci. Data **5**: 180292. doi:10.1038/sdata.2018.292

Appling, A. P., R. O. Hall, C. B. Yackulic, and M. Arroita. 2018*b*. Overcoming equifinality: Leveraging long time series for stream metabolism estimation. J. Geophys. Res. Biogeo. **123**: 624–625. doi:10.1002/2017JG004140

Appling, A. P., R. O. Hall, M. Arroita, and C. B. Yackulic. 2018*c*. streamMetabolizer: Models for estimating aquatic photosynthesis and respiration. R package version 0. 10. 9. http://github.com/USGS-R/streamMetabolizer.

Battin, T. J., A. Wille, R. Psenner, and A. Richter. 2004. Large-scale environmental controls on microbial biofilms in high-alpine streams. Biogeosciences **1**: 159–171. doi:10.5194/bg-1-159-2004

Battin, T. J., K. Besemer, M. M. Bengtsson, A. M. Romani, and A. I. Packmann. 2016. The ecology and biogeochemistry of stream biofilms. Nat. Rev. Microbiol. **14**: 251–263. doi:10.1038/nrmicro.2016.15

Berggren, M., and P. A. del Giorgio. 2015. Distinct patterns of microbial metabolism associated to riverine dissolved organic carbon of different source and quality. J. Geophys. Res. Biogeo. **120**: 989–999. doi:10.1002/2015JG002963

Berghuijs, W. R., R. A. Woods, and M. Hrachowitz. 2014. A precipitation shift from snow towards rain leads to a decrease in streamflow. Nat. Clim. Chang. **4**: 583–586. doi:10.1038/NCLIMATE2246

Bernhardt, E. S., J. B. Heffernan, N. B. Grimm, and others. 2018. The metabolic regimes of flowing waters. Limnol. Oceanogr. **63**: S99–S118. doi:10.1002/lno.10726

Biggs, B. J. F., R. A. Smith, and M. J. Duncan. 1999. Velocity and sediment disturbance of periphyton in headwater streams: Biomass and metabolism. J. North Am. Benthol. Soc. **18**: 222–241. doi:10.2307/1468462

Blaszczak, J. R., J. M. Delesantro, D. L. Urban, M. W. Doyle, and E. S. Bernhardt. 2019. Scoured or suffocated: Urban stream ecosystems oscillate between hydrologic and dissolved oxygen extremes. Limnol. Oceanogr. **64**: 877–894. doi:10.1002/lno.11081

Boix Canadell, M., N. Escoffier, A. J. Ulseth, S. N. Lane, and T. J. Battin. 2019. Alpine glacier shrinkage drives shift in dissolved organic carbon export from quasi-chemostasis to transport limitation. Geophys. Res. Lett. **46**: 8872–8881. doi:10.1029/2019gl083424

Bond, N. R., and B. J. Downes. 2003. The independent and interactive effects of fine sediment and flow on benthic invertebrate communities characteristic of small upland streams. Freshw. Biol. **48**: 455–465. doi:10.1046/j.1365-2427.2003.01016.x

Brown, L. E., D. M. Hannah, and A. M. Milner. 2003. Alpine stream habitat classification: An alternative approach incorporating the role of dynamic water source contributions. Arctic. Antarct. Alp. Res. **35**: 313–322 doi: 10.1657/1523-0430(2003)035[0313:ASHCAA]2.0.CO;2.

Brown, L. E., A. M. Milner, and D. M. Hannah. 2007. Groundwater influence on alpine stream ecosystems. Freshw. Biol. **52**: 878–890. doi:10.1111/j.1365-2427.2007.01739.x

Carbonneau, P. E., S. N. Lane, and N. E. Bergeron. 2004. Catchment-scale mapping of surface grain size in gravel bed rivers using airborne digital imagery. Water Resour. Res. **40**: 1–11. doi:10.1029/2003WR002759

Cauvy-Fraunié, S., P. Andino, R. Espinosa, R. Calvez, D. Jacobsen, and O. Dangles. 2016. Ecological responses to experimental glacier-runoff reduction in alpine rivers. Nat. Commun. **7**: 1–7. doi:10.1038/ncomms12025

Church, M. 2006. Bed material transport and the morphology of alluvial river channels. Annu. Rev. Earth Planet. Sci. **34**: 325–354. doi:10.1146/annurev.earth.33.092203.122721

Demars, B. O. L., and J. R. Manson. 2013. Temperature dependence of stream aeration coefficients and the effect of water turbulence: A critical review. Water Res. **47**: 1–15. doi:10.1016/j.watres.2012.09.054

Dietrich, J. T. 2017. Bathymetric structure-from-motion: Extracting shallow stream bathymetry from multi-view stereo photogrammetry. Earth Surf. Process. Landforms **42**: 355–364. doi:10.1002/esp.4060

Dodds, W. K., K. Gido, M. R. Whiles, M. D. Daniels, and B. P. Grudzinski. 2015. The stream biome gradient concept: Factors controlling lotic systems across broad biogeographic scales. Freshw. Sci. **34**: 1–19. doi:10.1086/679756

Duncan, M. J., A. M. Suren, and S. L. Brown. 1999. Assessment of streambed stability in steep, bouldery streams: Development of a new analytical technique. J. North Am. Benthol. Soc. **18**: 445–456. doi:10.2307/1468377

Enquist, B. J., E. P. Economo, T. E. Huxman, A. P. Allen, D. D. Ignace, and J. F. Gillooly. 2003. Scaling metabolism from organisms to ecosystems. Nature **423**: 639–642. doi:10.1038/nature01671

Eriksson, L., T. Byrne, E. Johansson, J. Trygg, and C. Vikström. 2006. Multi- and megavariate data analysis, basic principles and applications.

Gabbud, C., M. Bakker, M. Clémençon, and S. N. Lane. 2019. Hydropower flushing events cause severe loss of macrozoobenthos in Alpine streams. Water Resour. Res. **55**: 10056–10081. doi:10.1029/2019WR024758

Garcia, H. E., and L. I. Gordon. 1992. Oxygen solubility in seawater: Better fitting equations. Limnol. Oceanogr. **37**: 1307–1312. doi:10.4319/lo.1992.37.6.1307

Gordon, N. D., T. A. McMahon, B. L. Finlayson, C. J. Gippel, and R. J. Nathan. 2004. Stream hydrology: An introduction for ecologists. Chichester: John Wiley.

Guasch, H., J. Armengol, E. Martí, and S. Sabater. 1998. Diurnal variation in dissolved oxygen and carbon dioxide in two low-order streams. Water Res. **32**: 1067–1074. doi:10.1016/S0043-1354(97)00330-8

Hall, R. O., C. B. Yackulic, T. A. Kennedy, M. D. Yard, E. J. Rosi-Marshall, N. Voichick, and K. E. Behn. 2015. Turbidity, light, temperature, and hydropeaking control primary productivity in the Colorado River, Grand Canyon. Limnol. Oceanogr. **60**: 512–526. doi:10.1002/lno.10031

Horgby, Å., M. Boix Canadell, A. J. Ulseth, T. W. Vennemann, and T. J. Battin. 2019. High-resolution spatial sampling identifies groundwater as driver of CO_2 dynamics in an Alpine stream network. J. Geophys. Res. Biogeo. **124**: 1961–1976. doi:10.1029/2019JG005047

Hoyle, J. T., C. Kilroy, D. M. Hicks, and L. Brown. 2017. The influence of sediment mobility and channel geomorphology on periphyton abundance. Freshw. Biol. **62**: 258–273. doi:10.1111/fwb.12865

Huss, M., and R. Hock. 2018. Global-scale hydrological response to future glacier mass loss. Nat. Clim. Chang. **8**: 135–140 doi:s41558-017-0049-x.

Hyndman, R., G. Athanasopoulos, C. Bergmeir, G. Caceres, L. Chhay, M. O'Hara-Wild, F. Petropoulos, S. Razbash, E. Wang, and F. Yasmeen. 2019. forecast: Forecasting functions for time series and linear models. R package version 8.9. http://pkg.robjhyndman.com/forecast.

IPCC, 2019: Summary for policymakers. In: IPCC special report on the ocean and cryosphere in a changing climate [H.-O. Pörtner, D.C. Roberts, V. Masson-Delmotte, P. Zhai, M. Tignor, E. Poloczanska, K. Mintenbeck, M. Nicolai, A. Okem, J. Petzold, B. Rama, N. Weyer (eds.)]. In press.

Julian, J. P., M. W. Doyle, S. M. Powers, E. H. Stanley, and J. A. Riggsbee. 2008. Optical water quality in rivers. Water Resour. Res. **44**: 1–19. doi:10.1029/2007WR006457

Katz, S. B., C. Segura, and D. R. Warren. 2018. The influence of channel bed disturbance on benthic chlorophyll a: A high resolution perspective. Geomorphology **305**: 141–153. doi:10.1016/j.geomorph.2017.11.010

Killick, R., K. Haynes and I. A. Eckley. 2016. Changepoint: An R package for changepoint analysis. R package version 2.2.2. https://CRAN.R-project.org/package=changepoint.

Koenker, R. 2019. quantreg: Quantile Regression. R package version 5.51. https://CRAN.R-project.org/package=quantreg.

Lane, S. N., and P. W. Nienow. 2019. Decadal-scale climate forcing of Alpine glacial hydrological systems. Water Resour. Res. **55**: 2478–2492. doi:10.1029/2018WR024206

Lane, S. N., K. S. Richards, and J. H. Chandler. 1996. Discharge and sediment supply controls on erosion and deposition in a dynamic alluvial channel. Geomorphology **15**: 1–15. doi:10.1016/0169-555X(95)00113-J

Lane, S. N., M. Bakker, C. Gabbud, N. Micheletti, and J.-N. Saugy. 2017. Sediment export, transient landscape response and catchment-scale connectivity following rapid climate warming and Alpine glacier recession. Geomorphology **277**: 210–227. doi:10.1016/j.geomorph.2016.02.015

Malard, F., U. Uehlinger, R. Zah, and K. Tockner. 2006. Flood-pulse and riverscape dynamics in a braided glacial river. Ecology **87**: 704–716. doi:10.1890/04-0889

Mao, L., and M. A. Lenzi. 2007. Sediment mobility and bedload transport conditions in an alpine stream. Hydrol. Process. **21**: 1882–1891. doi:10.1002/hyp.6372

Mevik, B. H., R. Wehrens, and K. H. Liland. 2019. pls: Partial least squares and principal component regression. R package version 2.7-1. https://CRAN.R-project.org/package=pls

Milner, A. M., K. Khamis, T. J. Battin, and others. 2017. Glacier shrinkage driving global changes in downstream systems. Proc. Natl. Acad. Sci. **114**: 9770–9778. 201619807. doi:10.1073/pnas.1619807114

Montgomery, D. R., and J. M. Buffington. 1997. Channel-reach morphology in mountain drainage basins. Geol. Soc. Am. Bull. **109**: 596–611 doi:10.1130/0016-7606(1997)109<0596:CRMIMD>2.3.CO;2.

Naegeli, M. W., and U. Uehlinger. 1997. Contribution of the hyporheic zone to ecosystem metabolism in a prealpine gravel-bed-river. J. North Am. Benthol. Soc. **16**: 794–804. doi:10.2307/1468172

Peterson, C. G., A. C. Weibel, N. B. Grimm, and S. G. Fisher. 1994. Mechanisms of benthic algal recovery following spates: Comparison of simulated and natural events. Oecologia **98**: 280–290. doi:10.1007/BF00324216

Rasmussen, J. J., A. Baattrup-Pedersen, T. Riis, and N. Friberg. 2011. Stream ecosystem properties and processes along a temperature gradient. Aquat. Ecol. **45**: 231–242. doi:10.1007/s10452-010-9349-1

Raymond, P. A., C. J. Zappa, D. Butman, and others. 2012. Scaling the gas transfer velocity and hydraulic geometry in streams and small rivers. Limnol. Oceanogr. Fluids Environ. **2**: 41–53. doi:10.1215/21573689-1597669

Riley, A. J., and W. K. Dodds. 2013. Whole-stream metabolism: Strategies for measuring and modeling diel trends of dissolved oxygen. Freshw. Sci. **32**: 56–69. doi:10.1899/12-058.1

Roberts, B. J., P. J. Mulholland, and W. R. Hill. 2007. Multiple scales of temporal variability in ecosystem metabolism rates: Results from 2 years of continuous monitoring in a forested headwater stream. Ecosystems **10**: 588–606. doi:10.1007/s10021-007-9059-2

Robinson, C. T., U. Uehlinger, F. Guidon, P. Schenkel, and R. Skvarc. 2002. Limitation and retention of nutrients in alpine streams of Switzerland. SIL Proceedings1922-2010 **28**: 263–272. doi:10.1080/03680770.2001.11902585

Rode, M., A. J. Wade, M. J. Cohen, and others. 2016. Sensors in the stream: The high-frequency wave of the present. Environ. Sci. Technol. **50**: 10297–10307. doi:10.1021/acs.est.6b02155

Rott, E., M. Cantonati, L. Füreder, and P. Pfister. 2006. Benthic algae in high altitude streams of the Alps—A neglected component of the aquatic biota. Hydrobiologia **562**: 195–216. doi:10.1007/s10750-005-1811-z

Savoy, P., A. P. Appling, J. B. Heffernan, E. G. Stets, J. S. Read, J. W. Harvey, and E. S. Bernhardt. 2019. Metabolic rhythms in flowing waters: An approach for classifying river productivity regimes. Limnol. Oceanogr. **64**: 1835–1851. doi:10.1002/lno.11154

Schneider, J. M., D. Rickenmann, J. M. Turowski, K. Bunte, and J. W. Kirchner. 2015. Applicability of bed load transport models for mixed-size sediments in steep streams considering macro-roughness. Water Resour. Res. **51**: 5260–5283. doi:10.1002/2014WR016417

Schwendel, A. C., R. G. Death, and I. C. Fuller. 2010. The assessment of shear stress and bed stability in stream ecology. Freshw. Biol. **55**: 261–281. doi:10.1111/j.1365-2427.2009.02293.x

Segura, C., J. H. McCutchan, W. M. Lewis, and J. Pitlick. 2011. The influence of channel bed disturbance on algal biomass in a Colorado mountain stream. Ecohydrology **4**: 411–421. doi:10.1002/eco.142

Stoffel, M., and C. Corona. 2018. Future winters glimpsed in the Alps. Nat. Geosci. **11**: 458–460. doi:10.1038/s41561-018-0177-6

Tamburrino, A., and J. S. Gulliver. 2002. Free-surface turbulence and mass transfer in a channel flow. AIChE J. **48**: 2732–2743. doi:10.1002/aic.690481204

Thimijan, R., and R. Heins. 1983. Photometric, radiometric, and quantum light units of measure: A review of procedures for interconversion. Hortic. Sci. **18**: 818–822.

Uehlinger, U. 2000. Resistance and resilience of ecosystem metabolism in a flood-prone river system. Freshw. Biol. **45**: 319–332. doi:10.1046/j.1365-2427.2000.00620.x

Uehlinger, U., and M. W. Naegeli. 1998. Ecosystem metabolism, disturbance, and stability in a prealpine gravel bed river. J. North Am. Benthol. Soc. **17**: 165–178. doi:10.2307/1467960

Uehlinger, U., R. Zah, and H. Bürgi. 1998. The Val Roseg project: Temporal and spatial patterns of benthic algae in an Alpine stream ecosystem influenced by glacier runoff. IAHS-AISH Publ. **248**: 419–424.

Uehlinger, U., M. Naegeli, and S. G. Fisher. 2002. A heterotrophic desert stream? The role of sediment stability. West. North Am. Nat. **62**: 466–473.

Uehlinger, U., C. T. Robinson, M. Hieber, and R. Zah. 2010. The physico-chemical habitat template for periphyton in alpine glacial streams under a changing climate. Hydrobiologia **657**: 107–121. doi:10.1007/s10750-009-9963-x

Ulseth, A. J., R. O. Hall, M. Boix Canadell, H. L. Madinger, A. Niayifar, and T. J. Battin. 2019. Distinct air–water gas exchange regimes in low- and high-energy streams. Nat. Geosci. **12**: 259–263. doi:10.1038/s41561-019-0324-8

Vannote, R. L., G. W. Minshall, K. W. Cummins, J. R. Sedell, and C. E. Cushing. 1980. The river continuum concept. Can. J. Fish. Aquat. Sci. **37**: 130–137. doi:10.1139/f80-017

Vetsch, D., and others. 2018. System manuals of BASEMENT, Version 2.8. ETH Zurich: Laboratory of Hydraulics, Glaciology and Hydrology (VAW).

Ward, J. 1994. Ecology of alpine streams. Freshw. Biol. **32**: 277–294. doi:10.1111/j.1365-2427.1994.tb01126.x

Wellnitz, T. A., and J. V. Ward. 2000. Herbivory and irradiance shape periphytic architecture in a Swiss alpine stream. Limnol. Oceanogr. **45**: 64–75. doi:10.4319/lo.2000.45.1.0064

Wetzel, R. G. 2001. Light in inland waters, p. 49–69. *In* R. G. Wetzel [ed.], Limnology. Elsevier.

Zappa, C. J., W. R. McGillis, P. A. Raymond, J. B. Edson, E. J. Hintsa, H. J. Zemmelink, J. W. H. Dacey, and D. T. Ho. 2007. Environmental turbulent mixing controls on air-water gas exchange in marine and aquatic systems. Geophys. Res. Lett. **34**: L10601. doi:10.1029/2006GL028790

Acknowledgments

Financial support came from the Swiss Science Foundation (SNF, 200021_163015) to T. J. B. We want to thank Nicolas Escoffier, Amber Ulseth and Åsa Horgby for fieldwork and providing data, and Sébastien Ruettimann, Sophie Guignard, Valentin Sahli and Amin Niayifar for drone assistance and data processing.

Conflict of Interest

None declared.

Submitted 12 November 2019
Revised 29 July 2020
Accepted 14 November 2020

Associate editor: Bob Hall